



## THE INFLUENCE OF THERMO-MECHANICAL STRESS STATE ON THE TORQUE CAPACITY OF ROTATING INTERFERENCE FIT ASSEMBLY

### Alexandre Tácito Malavolta

Universidade Federal de São Carlos (UFSCar). Rodovia Washington Luís, km 235. São Carlos - SP – Brazil.  
malavolta@ufscar.br

### Sérgio Henrique Evangelista

Universidade Federal de São Carlos (UFSCar). Rodovia Washington Luís, km 235. São Carlos - SP – Brazil.  
toddyprof@ufscar.br

### Mariano Eduardo Moreno

Universidade Federal de São Carlos (UFSCar). Rodovia Washington Luís, km 235. São Carlos - SP – Brazil.  
mmoreno@ufscar.br

**Abstract.** *The interference fit assembly is a common type of coupling between rotating parts of machine elements like shafts and hubs. In general, conventional dimensioning of interference fit assembly takes into account only the stress state induced by the contact pressure between the outer shaft and inner hub radius. In the same way the determination of the torque capacity that can be transmitted by this assembly is based on resistant torque which is directly proportional to pressure magnitude, coefficient of friction and the surface areas in contact. However, additional stresses due to the centrifugal forces of the rotation and also temperature gradients can reduce the initial interference and hence decrease the torque capacity. Therefore this conventional dimensioning can be not safe or suitable to predict the torque capacity under operational conditions of machine elements. This work describes how to predict the admissible torque of interference fits considering a uniform angular speed and a steady state temperature field to represent these operational conditions. The Lamé's equations under isotropic linear elasticity assumption were used to derive the initial and additional stress state of the interference fit assembly. The analytical equations have provided the final interference and torque capacity after considering the additional thermo-mechanical effects. A typical problem is presented and the analytical results were compared with numerical results given by the finite element method. It can be observed that the conventional design approach becomes limited to predict the torque capacity in presence of additional thermo-mechanical stresses.*

**Keywords:** *interference fit, torque capacity, thermo-mechanical stress, finite element method, machine elements*

### 1. INTRODUCTION

The interference fits assembly or shrink fits are widely used in mechanical design. Many rotating machine elements like pulleys, gears, hubs, disks and bearings are mounted on shafts by using interference fit techniques. The main shrink fits advantage is the ability of transmit high torque and bending moments at low production costs.

In general, a conventional dimensioning of interference fit assembly takes into account only the stress state induced by the contact pressure between the outer shaft and inner hub radius. In the same way the determination of the torque capacity that can be transmitted by this assembly is based on resistant torque which is directly proportional to pressure magnitude, coefficient of friction and the surface areas in contact. However, additional stresses due to the centrifugal forces of the rotation and also temperature gradients can reduce the initial interference and hence decrease the torque capacity. Therefore this conventional dimensioning can be not safe or suitable to predict the torque capacity under operational conditions of machine elements.

Many authors have been studying the stress state generated in shrink fits under different assumptions of the shaft-hub geometry, thermo-mechanical loads and material behavior. Güven (1993) has investigated the stress states and the radial displacement of variable thickness hubs shrink fits considering the Tresca's yield criterion to describe the elastic-plastic behavior. However the author has not considerate the thermo-mechanical effects given by an angular rotating speed and thermal stresses. In work of Megahed and Abdel-Kader (1993) analytical equations are derivate considering the angular rotating speed effects to describe the stress state of shrink fits with a non-linear hardening material law. In others works numerical methods (like the finite element method - *FEM*) are applied to study the stress distribution in interference fits (Sen and Akasakal, 2004; Özel et al., 2005; Kovan, 2011).

Antoni (2013) has derived analytical equations to predict a safe operating domain and an optimum interference of shrink fits. The author considered an elastic-plastic material model and the thermo-mechanical effects given by the rotation and thermal stresses due to a uniform temperature variation. The results allow to determinate the rotation speed limit in which the radial stress decreases to zero on the interface contact or generates plasticity behavior. However the author does not present a wide discussion of the influence of the parameters involved neither the relation between the rotation speed and the torque capacity.

This work describes how to predict an admissible torque of interference fits under a uniform angular speed and a steady state heat flow loadings representing the operational conditions. Initially it presents the shrink fit problem with the main assumptions and hypothesis taken in account. Then, the analytical formulation is carried out considering the effects of interference, thermal stress and rotating loads. In a second part, the analytical formulation is applied to reach the shrink fit stress state and determinate the decrease of the torque capacity under different combinations of interference, uniform temperature variations and rotating speed levels. In this stage it is possible verify the influence of the additional stresses due to the centrifugal forces of the rotation and also temperature gradients. The results allow to determinate the reduction of the initial interference and hence the torque capacity decreasing. Finally it presents a typical problem and the analytical results are compared with numerical results given by the finite element method.

## 2. METHODOLOGY

The torque capacity determination is based on evolution of the radial stress state at the interface of the components which have been initially mounted with a known interference. Additional loads given by the rotating speed and thermal variations decrease the initial radial stress and hence decrease the pressure at the interface contacts area. The torque capacity becomes zero when the contact pressure reaches a null value.

A circular model representing a disk with plane stress assumption and a linear isotropic elastic material behavior is supposed at steady state condition to formulate the problem and generate the torque capacity evolution. The additional loads that decrease the initial stress state are taken in account by using the principle of superposition.

The theory of elasticity is applied to provide the equilibrium equations and the constitutive relations between stress and strain. Therefore the set of differential equations obtained are combined with the boundary conditions at the free tractions surfaces and at the contact interface surface and then solved. The equations results provide the evolution of the torque capacity with the additional thermo-mechanical loads.

### 2.1 Problem description

To develop the analytical formulation, the geometry of shrink fit will be represented by an assembly composed of two hollow cylinders as shown in Fig. 1. The inner solid denoted as (1) represents the shaft and the outer solid denoted as (2) the hub. After the interference mounting the solids are in equilibrium and (1) has an inner radius  $R_i$  and an interface radius  $R_c$  and (2) presents an inner radius  $R_c$  and the outer  $R_e$ .

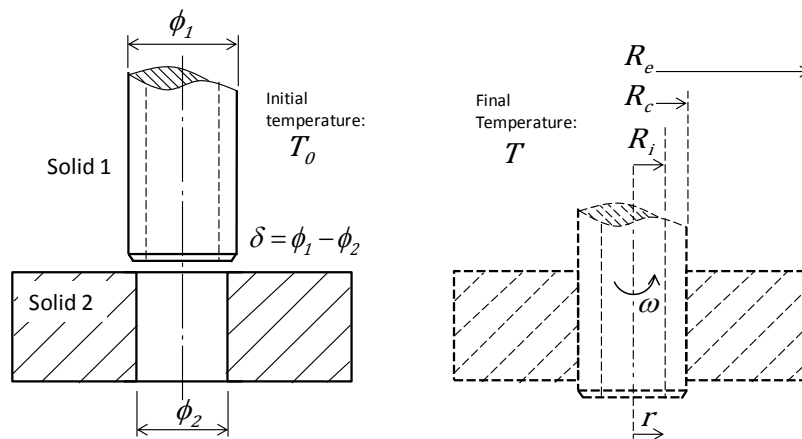


Figure 1. Schematic interference fit geometry

### 2.2 Stress state due to interference fit and thermal loading

The determination of the stress state generated by an interference fit between the shaft and the hub is a well-known problem (Timoshenko, 1980; Norton, 2011). The contact pressure on the interface ( $r = R_c$ ) considering only the initial interference is given by:

$$p_0 = \frac{0.5\delta}{\frac{R_c}{E_2} \left( \frac{R_e^2 + R_c^2}{R_e^2 - R_c^2} + \nu_2 \right) + \frac{R_c}{E_1} \left( \frac{R_c^2 + R_i^2}{R_c^2 - R_i^2} - \nu_1 \right)} \quad (1)$$

where  $\delta$  is the total diametral interference and  $E_k$ ,  $\nu_k$  ( $k = 1, 2$ ) are, respectively, the Young's module and Poisson's ratio of the solids (1) and (2).

However, in order to consider the temperature effects it is assumed a contact pressure variation  $\Delta p(T)$  due to the thermal expansions of the solids. This variation can increase or decrease the initial interference pressure  $p_0$ . A positive value of  $\Delta p$  indicates an increase of the initial interference pressure and, on the other way, the negative value a decrease. The Eq. (2) provides the pressure variation due to thermal effects.

$$\Delta p(T) = \frac{(\alpha_1 - \alpha_2)(T - T_0)}{\frac{1}{E_2} \left( \frac{R_e^2 + R_c^2}{R_e^2 - R_c^2} + \nu_2 \right) + \frac{1}{E_1} \left( \frac{R_c^2 + R_i^2}{R_c^2 - R_i^2} - \nu_1 \right)} \quad (2)$$

where  $(T - T_0)$  represents a uniform temperature variation and  $\alpha_k$  ( $k = 1, 2$ ) is the thermal expansion coefficient. The total interface pressure  $p$  will be given by:

$$p = p_0 + \Delta p(T) \quad (3)$$

Finally, since the total interface pressure is known, it is possible to determinate both radial stress  $\sigma_{r_0}$  and hoop stress  $\sigma_{\theta_0}$  distributions across the (1) and (2) solids as function of their radius and pressure load (Timoshenko, 1980).

$$\begin{aligned} \sigma_{r_0}^{(1)} &= -\frac{p R_c^2}{R_c^2 - R_i^2} \left( 1 - \frac{R_i^2}{r^2} \right) & R_i \leq r \leq R_c \\ \sigma_{r_0}^{(2)} &= \frac{p R_c^2}{R_e^2 - R_c^2} \left( 1 - \frac{R_e^2}{r^2} \right) & R_c \leq r \leq R_e \end{aligned} \quad (4)$$

### 2.3 Stress state due to rotating loading

As previously mentioned, the rotating load represents an additional stress state that decreases the initial radial stress given by Eq. (4). According to Johnson and Mellor (1970), the determination of this stress state is given by the radial equilibrium forces and has to comply with Eq. (5):

$$\frac{\partial \sigma_r}{\partial r} + \frac{(\sigma_r - \sigma_\theta)}{r} + \rho r \omega^2 = 0 \quad (5)$$

where  $\rho$  is the mass per unit volume and  $\omega$  the constant angular rotating speed. Considering the plane stress state and linear isotropic elasticity, the Hooke's law provides:

$$\begin{aligned} \sigma_r &= \frac{E}{1 - \nu^2} (\varepsilon_\theta + \nu \varepsilon_r) = \frac{E}{1 - \nu^2} \left( \frac{u}{r} + \nu \frac{du}{dr} \right) \\ \sigma_\theta &= \frac{E}{1 - \nu^2} (\nu \varepsilon_\theta + \varepsilon_r) = \frac{E}{1 - \nu^2} \left( \nu \frac{u}{r} + \frac{du}{dr} \right) \end{aligned} \quad (6)$$

Substituting Eq. (6) in Eq. (5) it is found the differential equation in terms of the radial displacement  $u$ :

$$r^2 \frac{d^2 u}{dr^2} + r \frac{du}{dr} - u + \left( \frac{1 - \nu^2}{E} \right) \rho \omega^2 r^3 = 0 \quad (7)$$

The solution of the Eq. (7) provides the radial displacement  $u$  to the solids (1) and (2):

$$\begin{aligned} u^{(1)} &= A_1 r + \frac{B_1}{r} - \left( \frac{1 - \nu_1^2}{8E_1} \right) \rho_1 \omega^2 r^3 & R_i \leq r \leq R_c \\ u^{(2)} &= A_2 r + \frac{B_2}{r} - \left( \frac{1 - \nu_2^2}{8E_2} \right) \rho_2 \omega^2 r^3 & R_c \leq r \leq R_e \end{aligned} \quad (8)$$

where  $A_k$  and  $B_k$  ( $k = 1, 2$ ) are constants. The radial stress  $\sigma_r$  to the solids (1) and (2) can be obtained substituting the Eq. (8) in Eq. (6):

$$\begin{aligned} \sigma_r^{(1)} &= \frac{E_1}{1 - \nu_1^2} \left[ A_1 (1 + \nu_1) + \frac{B_1}{r^2} (\nu_1 - 1) - \left( \frac{1 - \nu_1^2}{8E_1} \right) (3 + \nu_1) \rho_1 \omega^2 r^2 \right] & R_i \leq r \leq R_c \\ \sigma_r^{(2)} &= \frac{E_2}{1 - \nu_2^2} \left[ A_2 (1 + \nu_2) + \frac{B_2}{r^2} (\nu_2 - 1) - \left( \frac{1 - \nu_2^2}{8E_2} \right) (3 + \nu_2) \rho_2 \omega^2 r^2 \right] & R_c \leq r \leq R_e \end{aligned} \quad (9)$$

For a complete radial stress state determination it is necessary to determinate the constants  $A_k$  and  $B_k$  ( $k = 1, 2$ ). It can be carried out considering the boundary conditions at the free tractions surfaces and at the interface surface according to Eq.(10) and Eq.(11) respectively:

Alexandre T. Malavolta, Sérgio H. Evangelista and Mariano E. Moreno  
The Influence of Thermo-mechanical Stress State on the Torque Capacity of Rotating Interference Fit Assembly

$$\begin{aligned}\sigma_r^{(1)}(R_i) &= 0 \\ \sigma_r^{(2)}(R_e) &= 0\end{aligned}\quad (10)$$

$$\begin{aligned}\sigma_r^{(1)}(R_c) &= \sigma_r^{(2)}(R_c) \\ u^{(1)}(R_c) &= u^{(2)}(R_c)\end{aligned}\quad (11)$$

By using the principle of superposition, the decreased radial stress state  $\sigma_{rf}^{(k)}$  including the rotating load becomes:

$$\sigma_{rf}^{(k)} = \sigma_{r_0}^{(k)} + \sigma_r^{(k)} \quad k = 1,2 \quad (12)$$

At the interface surface ( $r = R_c$ ) the decreased contact pressure due to the rotating load is defined as:

$$\Delta p(\omega) = -\sigma_{rf}^{(1)} = -\sigma_{rf}^{(2)} \quad (13)$$

Finally, by using the principle of superposition, the total pressure at contact interface taking into account the effects of the press mounting, temperature changes and rotation loads is given by:

$$p_f = p_0 + \Delta p(T) + \Delta p(\omega) \quad (14)$$

## 2.4 Torque capacity

According to Norton (2011) the torque that can be transmitted by the shrink fit is define in terms of the pressure at the interface, which generates a friction force. The Eq. (15) presents this conventional torque capacity:

$$\hat{T} = 2\pi R_c^2 \mu L p_0 \quad (15)$$

where  $\mu$  is static coefficient of friction and  $L$  is the length of the hub engagement.

The value of interface pressure remains constant in this conventional approach. However, to take in account the evolution of the torque capacity with the additional loads, the pressure  $p_0$  is replaced by the decreased pressure given by Eq. (14) and the torque capacity can be rewritten as:

$$T = 2\pi R_c^2 \mu L p_f \quad (16)$$

## 3. RESULTS AND DISCUSSION

In order to verify the radial stresses, the interface pressure and the torque capacity evolution given by previous equations, two cases are analyzed. The results presented here correspond to the simulation of an assembly with shaft and hub of same material subjected to rotation loading and without thermal gradients. Therefore the objective is to investigate the exclusive influence of the rotating speed on the radial stress state and torque capacity. The Tab. 1 presents the geometry parameters and material properties adopted for these cases. In both cases generic steel properties are used for hub and shaft as well as the same interference fit. The modified parameters were the internal radius of the hollow shaft and the interface radius of the assembly.

Table 1. Geometry and material properties values used on the numerical examples.

Geometry / material properties		Case A	Case B
Inner shaft radius	$R_i$	10 [mm]	20 [mm]
Interface radius	$R_c$	50 [mm]	100 [mm]
Outer hub radius	$R_e$	200 [mm]	200 [mm]
Length of the hub	$L$	10 [mm]	10 [mm]
Diametral interference	$\delta$	0.05 [mm]	0.05 [mm]
Young's module	$E_1 = E_2$	210 [GPa]	210 [GPa]
Poisson's ratio	$\nu_1 = \nu_2$	0.3 [-]	0.3 [-]
Mass density	$\rho_1 = \rho_2$	7850 [Kg/m3]	7850 [Kg/m3]
Coefficient of friction	$\mu$	0.15 [-]	0.15 [-]

The initial stress state considering the interference fit mounting effect isolated is plotted on Fig. 2 to case A and Fig. 3 to case B. The graphs show the radial stress state from  $r = R_i$  to  $r = R_e$ . It can be observed that at the interface position ( $r = R_c$ ) the initial pressure is approximately 47 [MPa] for case A and 19 [MPa] for case B. These initial values of pressure are then decreased by the additional rotating load.

The radial stress distribution under different levels of rotational speed is shown on Fig. 4 and Fig. 5 for case A and case B respectively. The stress distribution obtained agrees with the well known solution of pure rotating isotropic discs with constant thickness under plane stress assumption. In this case, when the materials of the shaft and hub are the same, the maximum radial stress is localized at position  $r = \sqrt{R_i R_e}$ .

The decreased radial stress distribution is plotted on Fig. 6 and Fig. 7 for the cases A and B respectively. These curves are obtained adding the initial stress state of interference and the radial stress state due to rotating load. Knowing the radial stress evolution at the interface position for different levels of rotating speeds, the torque capacity can be obtained by Eq. (16) to each rotational speed analyzed. The evolution of the torque capacity versus the rotating speed is plotted on Fig. 8 and Fig. 9 to cases A and B respectively. It can be noticed that case A has the maximum rotating speed of 6000 [rpm] approximately and the case B 4250 [rpm]. Rotational speeds above these values represent total loss of contact between the components.

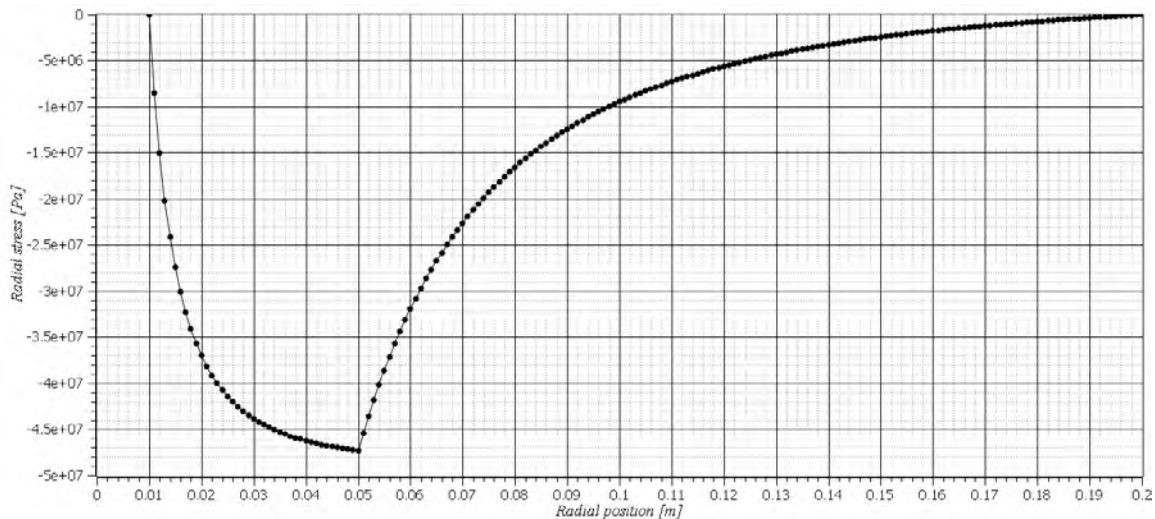


Figure 2. Radial stress  $\sigma_{r_0}^{(k)}$  [Pa] due to interference fit versus radial position [m] (case A).

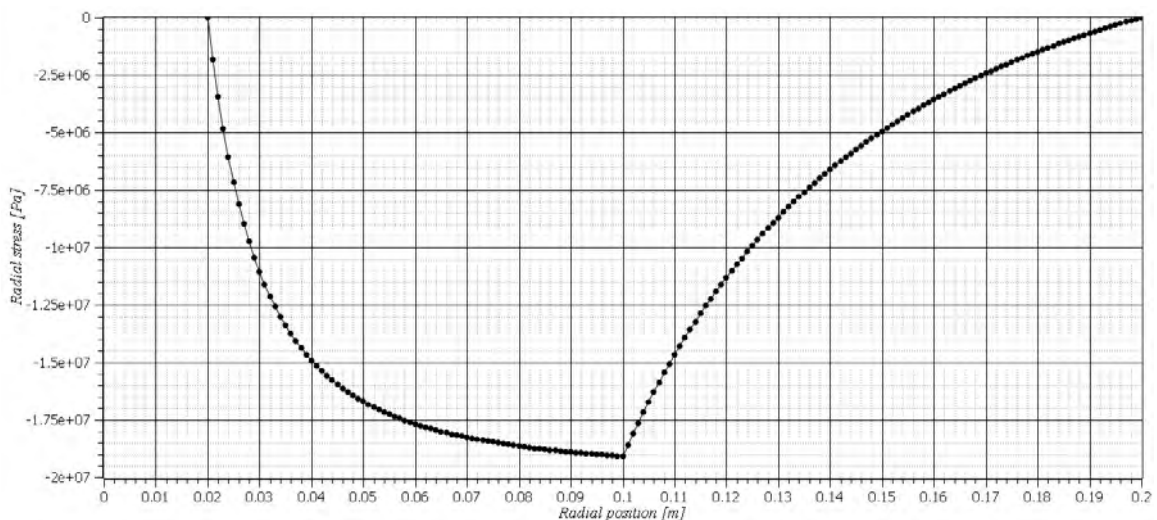


Figure 3. Radial stress  $\sigma_{r_0}^{(k)}$  [Pa] due to interference fit versus radial position [m] (case B).

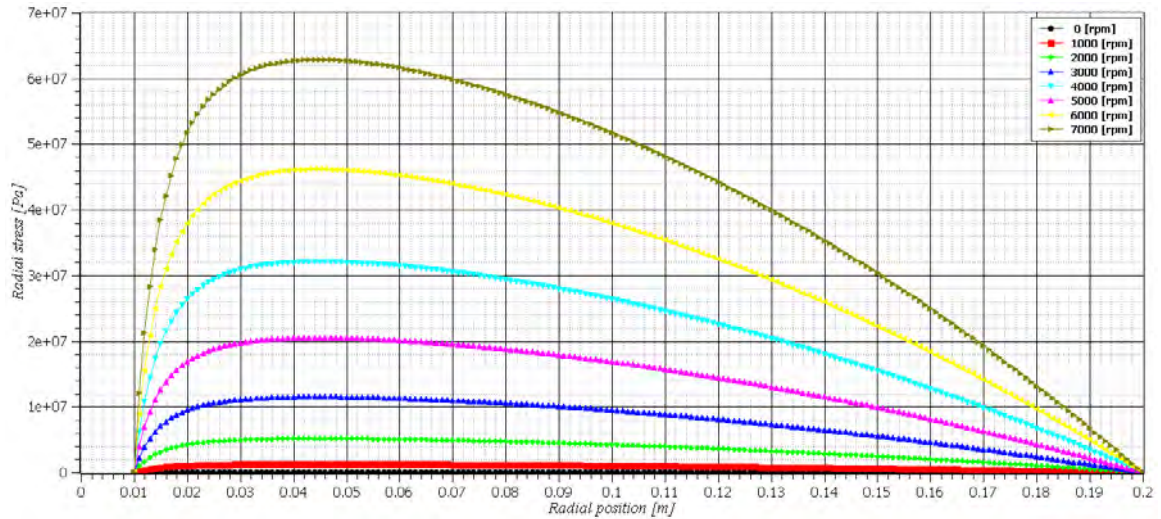


Figure 4. Radial stress  $\sigma_r^{(k)}$  [Pa] due to rotating load versus radial position [m] (case A).

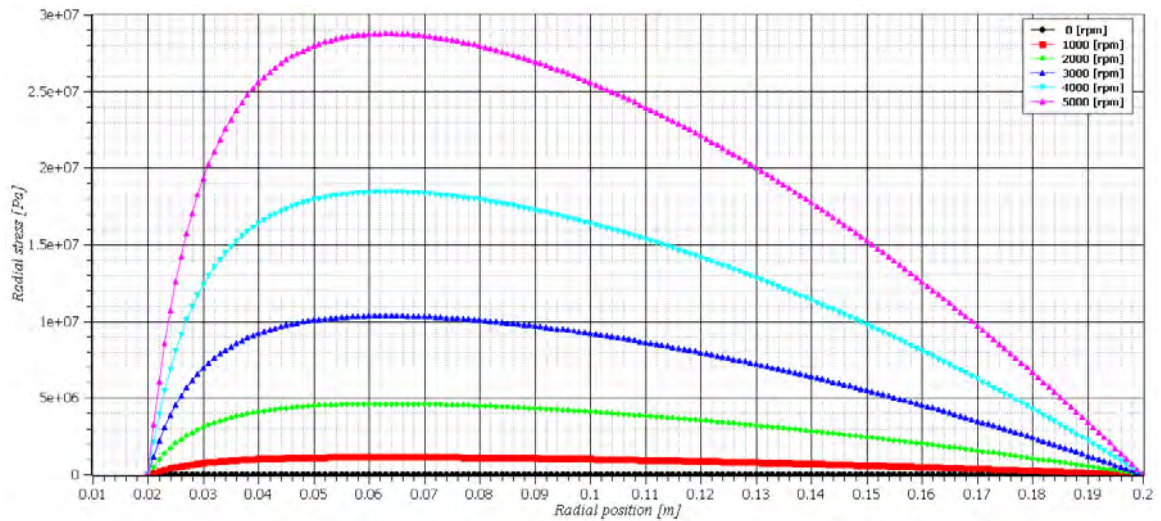


Figure 5. Radial stress  $\sigma_r^{(k)}$  [Pa] due to rotating load versus radial position [m] (case B).

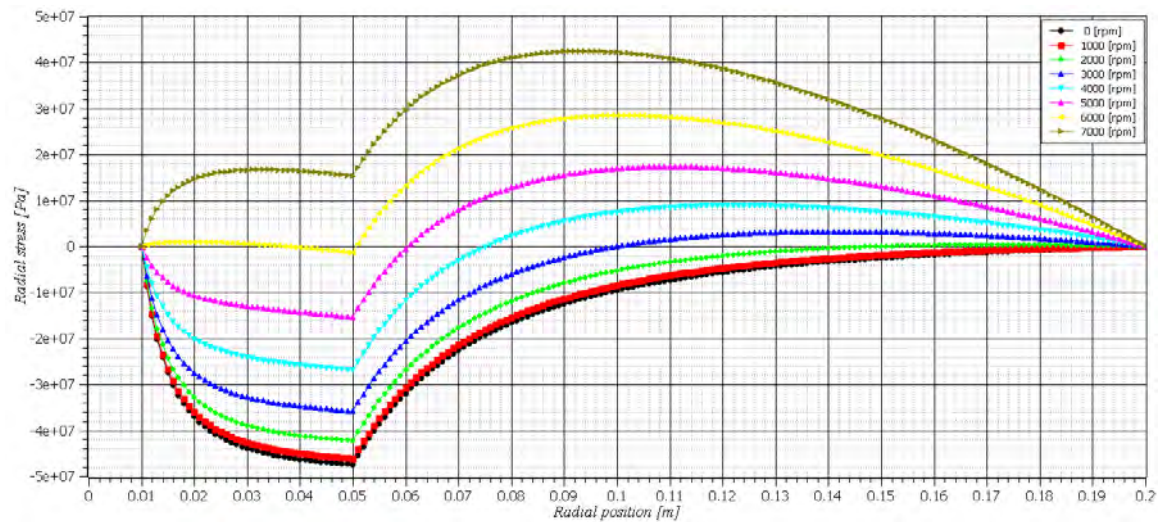


Figure 6. Decreased radial stress  $\sigma_{rf}^{(k)}$  [Pa] versus radial position [m] (case A).

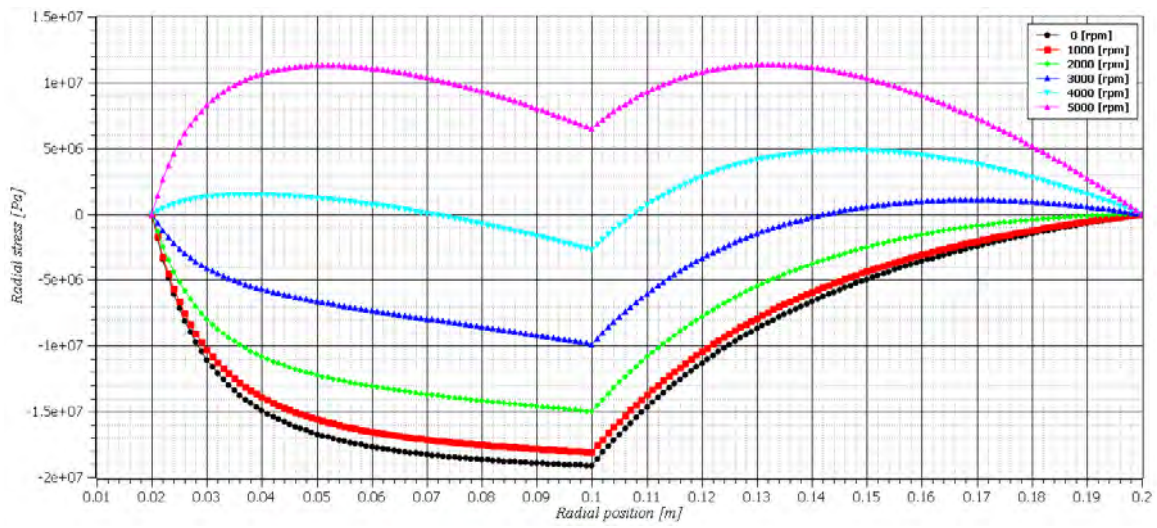


Figure 7. Decreased radial stress  $\sigma_{rf}^{(k)}$  [Pa] versus radial position [m] (case B).

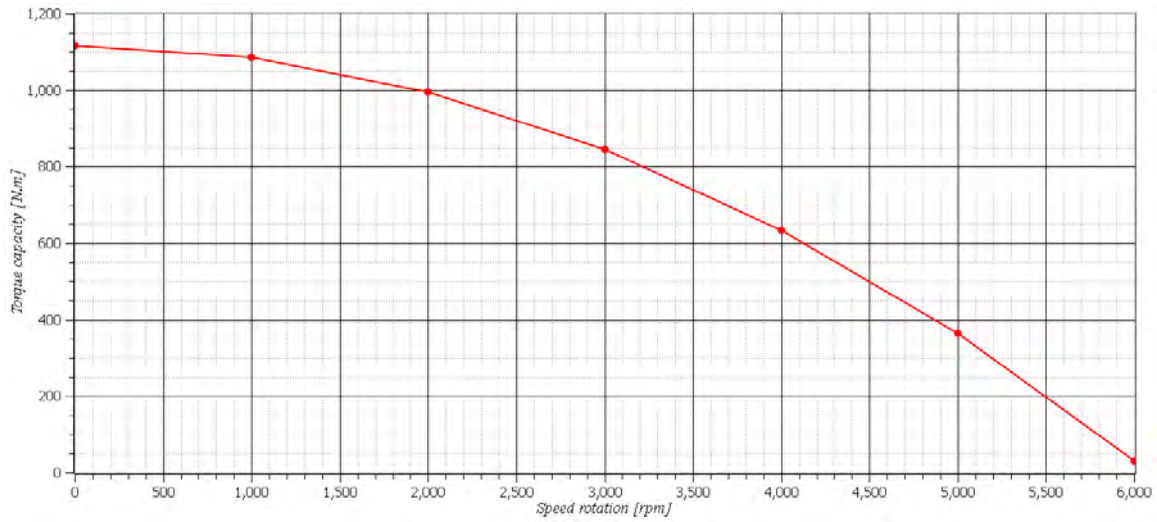


Figure 8. Torque capacity [N.m] versus rotating speed [rpm] (case A).

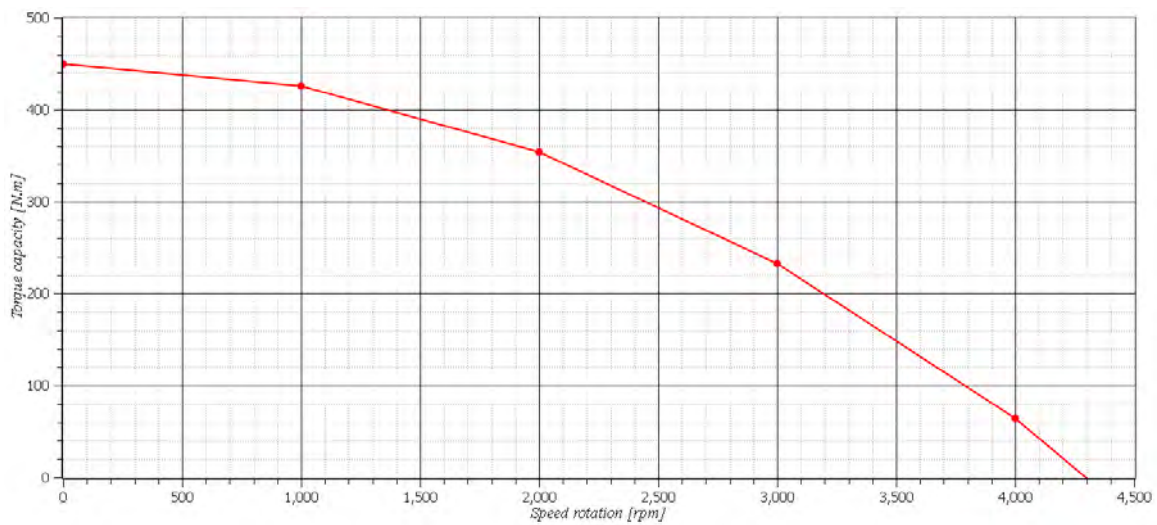


Figure 9. Torque capacity [N.m] versus rotating speed [rpm] (case B).

Additionally, in order to verify the radial stress state given by analytical results, a finite element model has generated. The model was created with shell elements under plane stress assumptions and considering an elastic linear isotropic material. The geometry parameters and material properties are chosen as the same as case B presented in Tab. 1. Coupling equations between the interface nodes of the shaft and hub were used to represent the initial interference fit and an inertial force is applied in order to represent the rotating load. The finite element model mesh is illustrated in Fig. 10 and Fig. 11 presents the radial stress distribution obtained on the hub to different levels of rotation speed.

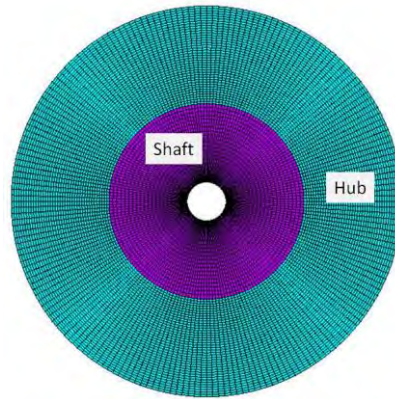


Figure 10. Finite element model mesh.

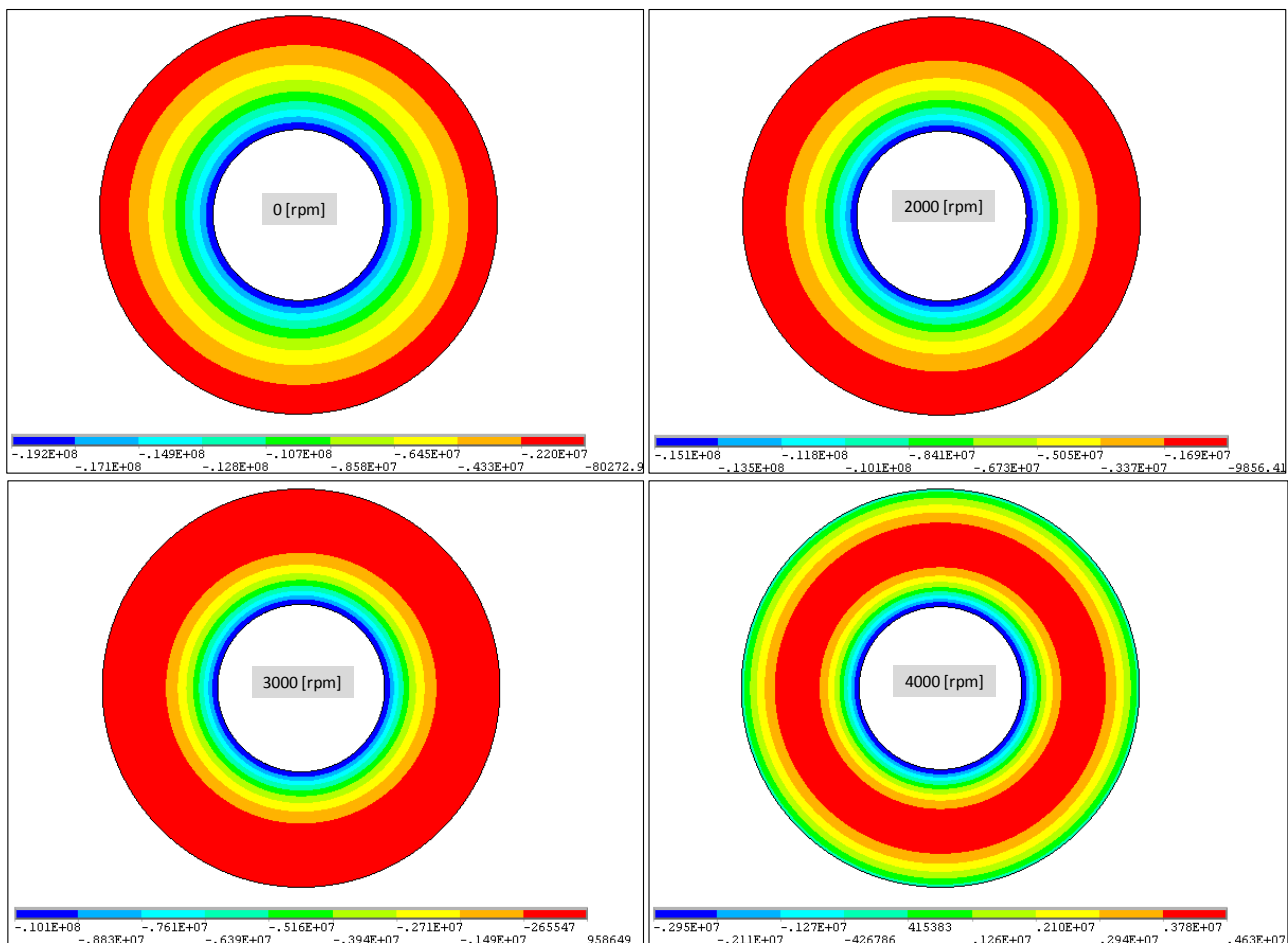


Figure 11. Distribution of the radial stress [Pa] on the hub at different rotating levels.

A comparison between analytical (given by Eq. 12) and numerical (given by finite element model) radial stresses is presented in Tab. 2. The Tab. 2 compares the radial stress at different radial position on the hub (from the interface radius until the outer radius) and to different rotation speed levels. It can be noticed that the numerical results agree with the analytical solution and the differences observed are reasonable.

22nd International Congress of Mechanical Engineering (COBEM 2013)  
November 3-7, 2013, Ribeirão Preto, SP, Brazil

Table 2. Comparison between analytical and numerical radial stresses on the hub.

Radial position [mm]	Radial stress [MPa]							
	Numerical	Analytical	Numerical	Analytical	Numerical	Analytical	Numerical	Analytical
100	-19.20	-19.09	-15.13	-15.00	-10.06	-9.89	-2.95	-2.73
120	-11.76	-11.31	-8.23	-7.78	-3.81	-3.36	2.37	2.83
140	-6.89	-6.62	-4.05	-3.78	-0.50	-0.24	4.47	4.73
160	-3.72	-3.58	-1.71	-1.57	0.81	0.95	4.33	4.47
180	-1.55	-1.49	-0.48	-0.43	0.85	0.91	2.71	2.77
200	-0.08	0.00	-0.01	0.00	0.08	0.00	0.20	0.00
	0		2000		3000		4000	
	Rotation speed [rpm]							

#### 4. CONCLUSION

The results provided by analytical formulation showed how the torque capacity of shrink fit mountings of machine elements can be decreased with additional loads. It can be observed that the conventional design approach becomes limited to predict the torque capacity in presence of additional thermo-mechanical stresses. The analytical results agreed with numerical results given by finite element model for the example developed in case (B).

The formulation can be adjusted by considering other effects like a non-uniform temperature variation across the radial position and others combinations of material properties and geometry. Therefore the study presented can be improved and used as pre-design tool of machine elements of interference mountings.

#### 5. REFERENCES

- Antoni, N., 2013. "Contact separation and failure analysis of a rotating thermo-elastoplastic shrink-fit assembly". *Applied Mathematical Modelling*, Vol. 37, n.4, p. 2352-2363.
- Güven, U., 1993. "Stress distribution in shrink fit with elastic-plastic hub exhibiting variable thickness". *International Journal of Mechanical Sciences*, Vol. 35, n.1, p. 39-46.
- Johnson, W. and Mellor, P. B., 1970. *Plasticity for mechanical engineers*. Van Nostrand, London, 3<sup>rd</sup> edition.
- Kovan, V., 2011. "Separation frequency analysis of interference fitted hollow shaft-hub connections by finite element method". *Advances in Engineering Software*, Vol. 42, n.9, p. 644-648.
- Megahed, M.M. and Abdel-Kader, M.S., 1993. "Elastoplastic analysis of rotating shrink-fitted discs with nonlinear hardening characteristics". *International Journal of Solids and Structures*, Vol. 30, n.6, p.751-765.
- Norton, R.L., 2011. *Machine design - an integrated approach*. Prentice-Hall, Boston, 4<sup>th</sup> edition.
- Özel, A.; Temis, S.; Aydin, M.D. and Sen, S., 2005. "Stress analysis of shrink-fitted joints for various fit forms via finite element method". *Material and Design*, Vol. 26, n.4, p. 281-289.
- Sen, S. and Akasakal, B., 2004. "Stress analysis of interference fitted shaft-hub system under transient heat transfer conditions". *Material and Design*, Vol. 25, n.5, p. 407-417.
- Timoshenko, S.P. and Goodier, J.N., 1980. *Teoria da elasticidade*. Guanabara Dois, Rio de Janeiro, 3<sup>rd</sup> edition.

#### 6. RESPONSIBILITY NOTICE

The authors are the only responsible for the printed material included in this paper.